We are IntechOpen, the world's leading publisher of Open Access books Built by scientists, for scientists

6,900
Open access books available

185,000
International authors and editors

200M
Downloads

Our authors are among the

154
Countries delivered to

TOP 1%
most cited scientists

12.2%
Contributors from top 500 universities



WEB OF SCIENCE™

Selection of our books indexed in the Book Citation Index in Web of Science™ Core Collection (BKCI)

Interested in publishing with us?
Contact book.department@intechopen.com

Numbers displayed above are based on latest data collected.
For more information visit www.intechopen.com



Chapter 2

Lithium Ferrite: Synthesis, Structural Characterization and Electromagnetic Properties

Sílvia Soreto, Manuel Graça, Manuel Valente and Luís Costa

Additional information is available at the end of the chapter

http://dx.doi.org/10.5772/110790

Abstract

Lithium ferrite ($LiFe_5O_8$) is a cubic ferrite, belongs to the group of soft ferrite materials with a square hysteresis loop, with high Curie temperature and magnetization. The spinel structure of $LiFe_5O_8$ has two crystalline forms: ordered, β-$LiFe_5O_8$ (*Fd3m* space group) and disordered, *α*-$LiFe_5O_8$ ($P4_132/P4_332$ space group). It has numerous technological applications in microwave devices, computer memory chip, magnetic recording, radio frequency coil fabrication, transformer cores, rod antennas, magnetic liquids among others. It is also a promising candidate for cathode in rechargeable lithium batteries. In this work, the dc electrical conductivity, the impedance spectroscopy and the magnetization of Li_2O-Fe_2O_3 powders, with [Li]/[Fe]=1/5 (mol), heat-treated at several temperatures, are studied and related to their structure and morphology. The structural data were obtained by X-ray diffraction and Raman spectroscopy, and the morphology by scanning electron microscopy. The impedance spectroscopy was analysed in function of temperature and frequency, and it was observed that the dielectric properties are highly dependent on the microstructure of the samples. The dc magnetic susceptibility was recorded with a vibrating sample magnetometer, under zero field cooled and field cooled sequences, between 5-300 K. Typical hysteresis curves were obtained and the saturation magnetization increases with increase in heat-treatment temperature.

Keywords: lithium ferrite, electric and dielectric properties, magnetic properties

1. Introduction

Technologically, ferrites are very important due to their interesting magnetic and electrical properties which can be exploited for applications in high-capacity batteries, electrochromic displays, wastewater cleaning, low magnetization ferrofluids, intercalation electrodes in

INTECH
open science | open minds

© 2017 The Author(s). Licensee InTech. This chapter is distributed under the terms of the Creative Commons Attribution License (http://creativecommons.org/licenses/by/3.0), which permits unrestricted use, distribution, and reproduction in any medium, provided the original work is properly cited. CC BY

rechargeable batteries and as strong oxidizing agents [1–5]. Ferrites crystallize in three structure: (i) cubic spinel structure with the general formula $MO.Fe_2O_3$ ($M = Mn^{2+}$, Fe^{2+}, Co^{2+}, Ni^{2+}, Cu^{2+}, Zn^{2+}, Mg^{2+}); (ii) hexagonal ferrites with the formula $MO.6Fe_2O_3$ ($M = Ba^{2+}$, Ca^{2+}, Sr^{2+}); and (iii) and garnets with the formula $2M_2O_3.5Fe_2O_3$ where M is a cation with (3+) charge such as Y or another rare earth [6].

The cubic lithium ferrite (**Figure 1**), spinel $LiFe_5O_8$ [7], is one of the most important ferrites, and it belongs to the soft ferrite materials group, with high Curie temperature (620°C) [8], square hysteresis loop and high magnetization. The spinel lithium ferrite has been widely studied and confirmed to have two crystalline forms: β-$LiFe_5O_8$ (*Fd3m* space group), known as the disordered $LiFe_5O_8$, and the α-$LiFe_5O_8$ (space group $P4_132/P4_332$), called ordered spinel phase. The first one is obtained by the rapid quenching of the samples from temperatures above 800°C to room temperature. Upon slow cooling and below 750°C, an ordered phase is obtained [9]. In the ordered form, α-$LiFe_5O_8$, the octahedral *12d* and tetrahedral *8c* sites are occupied by iron ions, Fe^{3+}, and the octahedral *4b* positions are occupied by lithium ions, Li^+, in the cubic primitive cell. The disordered structure, β-$LiFe_5O_8$, has an inverse spinel structure, where the tetrahedral *8a* positions are occupied by Fe^{3+} ions and the ions Li^+ and Fe^{3+} are randomly distributed over the *16d* octahedral positions [10, 11].

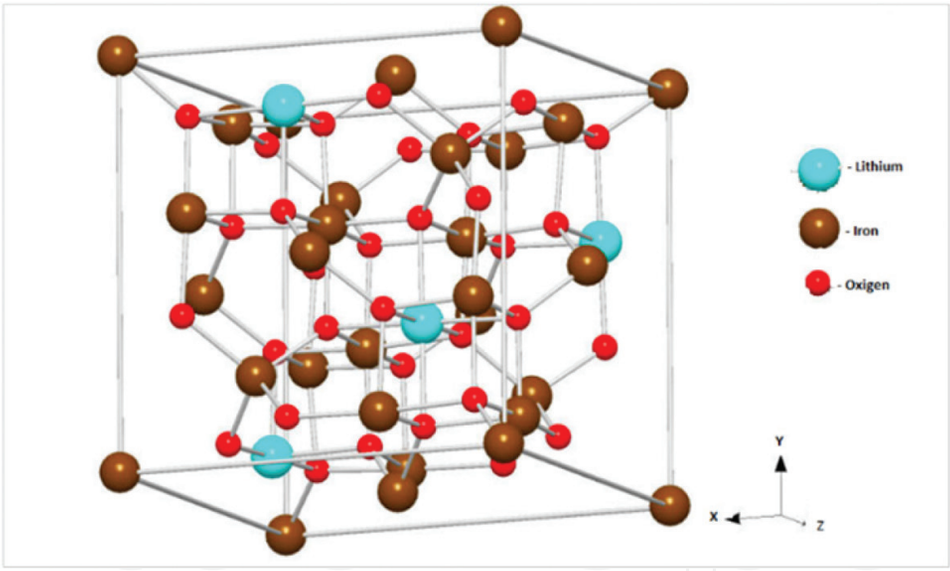


Figure 1. Cubic crystal of $LiFe_5O_8$ with space group P4132 (213).

To prepare $LiFe_5O_8$ by solid-state reaction method, high temperatures (>1200°C) are needed, which is a major issue due to the volatility of lithium above 1000°C. Therefore, the prepared material has a low quality because the sintering process normally leads to low specific surface areas [12], affecting its electrical and magnetic properties. Several chemical methods have been used for synthesis, such as co-precipitation, glass crystallization, hydrothermal, mechanical alloying and sol-gel methods. Therefore, the preparation of $LiFe_5O_8$ at low temperatures is a subject of interest.

In order to improve the material properties, in this work lithium ferrite was prepared at a low temperature, by the solid-state reaction method using iron and lithium nitrates as precursors. First, the use of nitrates as base materials and, second, the use of the high-energy planetary ball milling to prepare the base material for further heat treatments are not conventional route and denote improvements which have not been reported in the literature. The electric and magnetic properties of the ferrite prepared by this method have been already published [5, 13, 14]. With the main aim to enhance the electric and magnetic properties of $LiFe_5O_8$ and determine the best temperature for the thermal treatment, the powders after the ball milling are heat-treated at different temperatures.

The dependence of the particle size with the sintering temperature was also studied, and these studies were correlated with the measured electrical, dielectric and magnetic properties. The obtained results were analysed and compared with those presented in the literature.

2. Methods and procedures

As described in detail in our recent papers [5, 12, 13], the solid-state method was used to prepare lithium ferrite ($LiFe_5O_8$) powders starting with iron (III) nitrate ($Fe(NO_3)_3.9H_2O$) and lithium nitrate ($LiNO_3$ (Merck KGaA, Darmstadt, Germany). Considering the 1:5 required stoichiometry of Li:Fe, appropriate amounts of the two starting materials were mixed and homogenized in a planetary ball mill system (Fritsch Pulverisette 7.0) at 250 rpm for 1 h using equal volumes of balls to powders. Following this, 10 mL of ethanol was added to the mixture followed by additional ball milling at 500 rpm for 3 h, stopping the system for 5 min every hour to reduce over-heating. Next, in order to evaporate the ethanol, the vessel with the mixture was placed in a furnace at 80°C for 24 h.

The next step in the synthesis procedure was heat treatment of the powder at nine temperatures between 200 and 1400°C (see **Figure 2**) at 10°C/min in two steps: first at 100°C for 1 h and the second at desired temperature for 4 h. After this heat treatment, the samples were structurally characterized using the techniques of X-ray diffraction (XRD), micro-Raman spectroscopy and scanning electron microscopy (SEM). The equipment used for the structural characterization was X'Pert MPD Philips diffractometer (CuKα radiation, λ = 1.54060 Å) for X-ray diffraction, an HR-800-UV Jobin Yvon Horiba spectrometer (532 nm laser line) for micro-Raman spectroscopy using a microscope objective (50×) and a Hitachi S4100-1 SEM system for SEM images with the samples covered with carbon before microscopic observation. Further details on these procedures are given in Refs. [5, 12, 13]. Electrical and magnetic measurements on the samples were performed following the structural characterization.

For the measurements of electrical conductivity and impedance, the samples were pressed into 2-mm-thick discs with the opposite sides of the discs painted with silver paste for electrical contacts. The measurements were performed in helium atmosphere in order to improve the heat transfer and eliminate the moisture. The dc conductivity (σ_{dc}) was measured from 100 to 360 K employing a Keithley Model 617 electrometer using applied voltage of 100 V. Employing an Agilent 4294A precision impedance analyser in the Cp-Rp configuration, the measurements of impedance in the frequency range of 100 Hz–2 MHz were performed from 200 to 360 K.

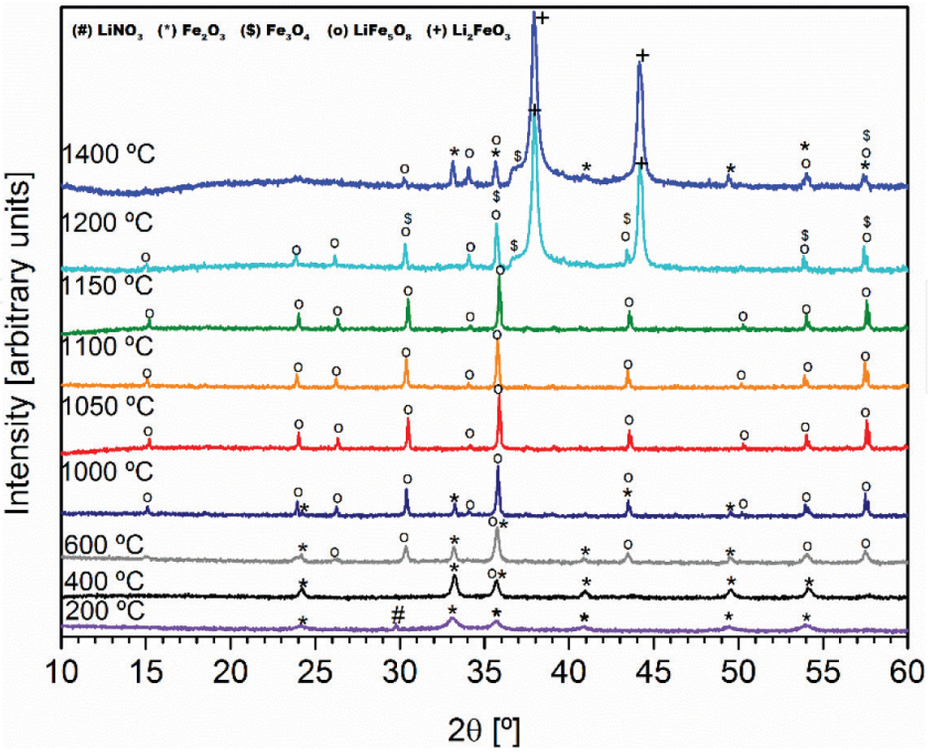


Figure 2. XRD patterns of the powders heat-treated between 400 and 1400°C: (*) Fe_2O_3; (o) $LiFe_5O_8$; (+) Li_2FeO_3; (#) $LiNO_3$. Adapted from Refs. [13, 14].

The magnetic properties of the samples were measured using a vibrating sample magnetometer (VSM). The dc magnetic susceptibility was measured from 5 to 300 K under two protocols: (i) cooling the sample in zero field (ZFC) and (ii) cooling the sample with the magnetic field applied (FC). Typical hysteresis curves were obtained at several temperatures.

3. Results and discussion

3.1. Structural and morphological measurements

Figure 2 shows the XRD patterns of the samples after each heat treatment. The XRD spectra of the sample treated at 200°C shows the presence of lithium nitrate crystal phase. This phase disappears with the increase in the heat-treatment temperature. The samples heat-treated at 200 and 400°C present the α-Fe_2O_3 as the major crystalline phase. The non-detection by the XRD of the lithium nitrate phase in the sample treated at 400°C suggests the existence of an amorphous phase containing mainly lithium ions. This result also revealed that the planetary ball milling process did not induce the formation of new crystalline phases before the heat treatments.

A low amount of lithium ferrite is found in the sample with heat treatment at 600°C, but the main diffraction peaks are attributed to the α-Fe_2O_3 phase. The formation of $LiFe_5O_8$ crystal phase can be attributed to the reaction between α-Fe_2O_3 and free Li^+ ions. In samples with heat

http://dx.doi.org/10.5772/110790

treatments at 1050, 1100 and 1150°C, all diffraction peaks can be assigned to the lithium ferrite crystal phase as described in Eq. (1) with loses of NO_x.

$$5Fe\left(NO_3\right)_3 + LiNO_3 \xrightarrow{\Delta} LiFe_5O_8 + y\,NO_x \tag{1}$$

In the sample treated at 1200°C besides lithium ferrite peaks, the lithium ferrate (Li_2FeO_3) phase is also detected. The presence of this phase can be explained through the chemical reaction, Eq. (2), where the peak characteristics of Fe_3O_4 are also present.

$$15\,Fe\left(NO_3\right)_3 + 3\,LiNO_3 \xrightarrow{\Delta} LiFe_5O_8 + Li_2FeO_3 + 3Fe_3O_4 + y\,NO_x \tag{2}$$

In the sample heat-treated at 1400°C, besides the peak characteristics of magnetite, lithium ferrite and lithium ferrate crystal phases also present peak characteristics of hematite, Eq. (3). In this sample, the major phase is attributed to lithium ferrate crystal phase showing broad diffraction peaks.

$$15\,Fe\left(NO_3\right)_3 + 3\;LiNO_3 \xrightarrow{\Delta} LiFe_5O_8 + Li_2FeO_3 + Fe_3O_4 + 3Fe_2O_3 + y\,NO_x \tag{3}$$

According to Wolska et al. [7] results, for heat treatment above 1000°C the disordered $LiFe_5O_8$ phase can be formed. However, in our results, the $LiFe_5O_8$ phase detected was only the ordered one (α-$LiFe_5O_8$) with the space group $P4_132$/$P4_332$.

To determine the crystallite size, L_c, of lithium ferrite crystal phase, the Debye-Scherrer equation was used:

$$L_c = \frac{N\lambda}{\beta\cos\theta} \tag{4}$$

Here, β is full width half maximum of the diffracted peaks, λ is the wavelength of X-ray radiation, θ is the angle of diffraction and N is a numerical factor frequently referred to as

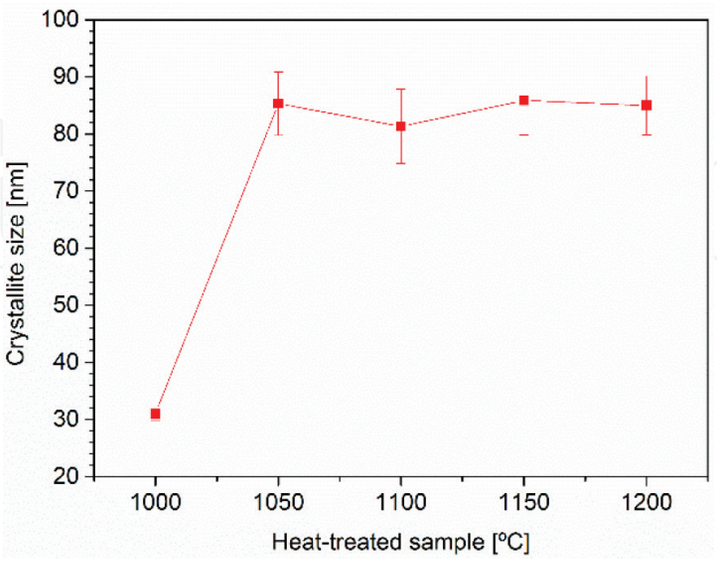


Figure 3. Crystallite size of $LiFe_5O_8$ phase in samples heat-treated at 1000, 1050, 1100, 1150 and 1200°C.

the crystallite-shape factor [15, 16] and being $N = 0.9$ a good approximation in the absence of detailed information [17].

Substituting the relevant data from XRD profile measurement, the average crystallite sizes and its errors bars are shown in **Figure 3**.

A crystallite size of about 85 nm was observed in the samples heat-treated at 1050, 1100, 1150°C, which only presents $LiFe_5O_8$ crystal phase, and in the sample heat-treated at 1200°C. The sample treated at 1000°C has the lowest crystallite size, 31 ± 1 nm.

The samples presenting $LiFe_5O_8$ as major crystal phase, that is, heat-treated at temperatures between 400 and 1400°C, were also analysed using Raman spectroscopy (**Figure 4**).

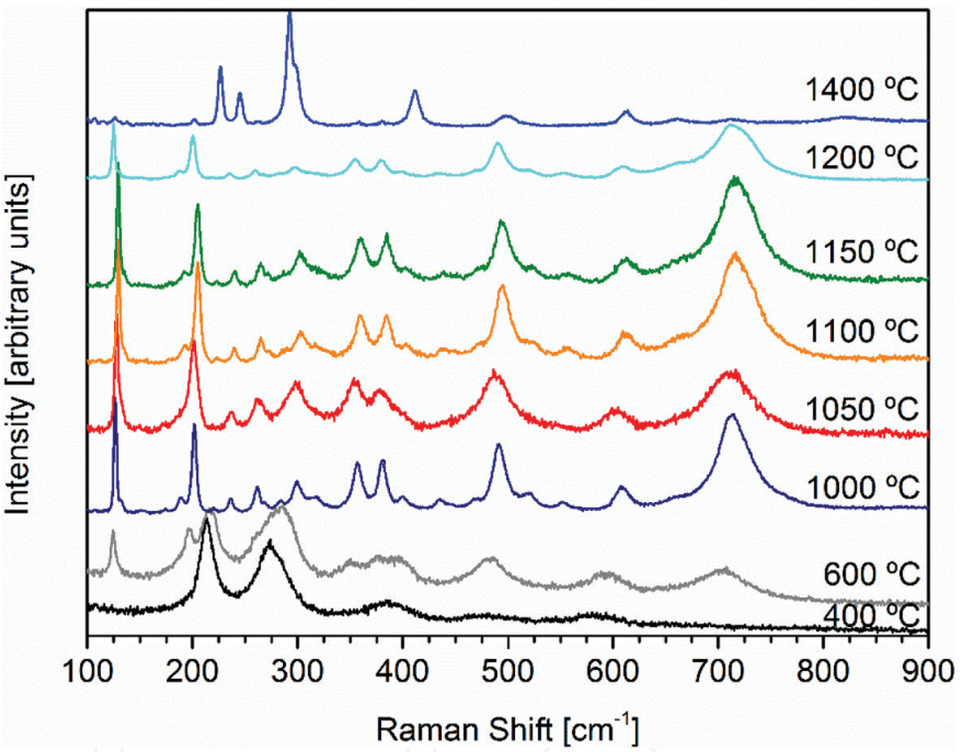


Figure 4. Raman spectra for the samples with heat treatments between 400 and 1400°C. Adapted from Refs. [13, 14].

According to the Raman spectroscopy spectra, all the samples show the vibration mode characteristic of both ordered and disordered lithium ferrite phases.

For the samples treated between 1000 and 1400°C, the vibrational peaks at 199–206 and 237–241 cm^{-1} indicate the presence of the ordered α-$LiFe_5O_8$ phase [18]. All the vibrational peaks of the $LiFe_5O_8$ phase are given in **Table 1**. In the samples heat-treated at 600, 1000 and 1400°C, besides the vibrational modes that mark the presence of lithium ferrite, the vibrational mode characteristic of α-Fe_2O_3 is also present [19].

According to the Raman spectra, for the sample heat-treated at 1200°C and crossing with the XRD results, we can infer about the vibration modes of the lithium ferrate (Li_2FeO_3). The

http://dx.doi.org/10.5772/110790

Sample								Assigned to
400°C	**600°C**	**1000°C**	**1050°C**	**1100°C**	**1150°C**	**1200°C**	**1400°C**	
						125	125	Li_2FeO_3
	126	126	128	130	130			$LiFe_5O_8$
							137	α-Fe_2O_3
		170	170	170	172	171		$LiFe_5O_8$
						188		Fe_3O_4 [19]
		195		196	195			$LiFe_5O_8$
	199	202	201	206	206	201	202	α-$LiFe_5O_8$ [7, 18]
214	217		B					α-Fe_2O_3 [19]
		223	220	226	221		226	$LiFe_5O_8$
		237	239	241	241	239	245	α-$LiFe_5O_8$ [7, 18]
		263	267	266	267	262	262	α-$LiFe_5O_8$ [7, 18] β-$LiFe_5O_8$ [7, 18]
274	287	286					292	α-Fe_2O_3 [19]
						298	298	Fe_3O_4 [19]
		300	301	306	305	301		α-$LiFe_5O_8$ [6, 17] β-$LiFe_5O_8$ [7]
		320						α-$LiFe_5O_8$ [7, 18] β-$LiFe_5O_8$ [7, 18]
	353	358	358	361	362	357	357	α-$LiFe_5O_8$ [7, 18] β-$LiFe_5O_8$ [7, 18]
388	379	383	382	386	385	382	380	α-$LiFe_5O_8$ [7, 18] β-$LiFe_5O_8$ [7, 18]
	400	405		407	410	409	410	α-$LiFe_5O_8$ [7, 18] β-$LiFe_5O_8$ [7, 18]
						437		Li_2FeO_3
		439		438	441			α-$LiFe_5O_8$ [7, 18] β-$LiFe_5O_8$ [7, 18]
		475		475	475	473		α-$LiFe_5O_8$ [7, 18] β-$LiFe_5O_8$ [7, 18]
486	489	492	492	496	496	494	498	α-$LiFe_5O_8$ [7, 18] β-$LiFe_5O_8$ 7, 18]
		523		526	526	523		$LiFe_5O_8$
		555		560	558	558		α-$LiFe_5O_8$ 7, 18] β-$LiFe_5O_8$ [7, 18]
590								not identified
	603							not identified
		611	610	612	614	612	613	α-$LiFe_5O_8$ [7, 18] β-$LiFe_5O_8$ [7, 18]
		663		660	660		661	α-$LiFe_5O_8$ [7, 18]
						668		Fe_3O_4 [19]
	707	715	719	719	719	718		α-$LiFe_5O_8$ [7, 18] β-$LiFe_5O_8$ [7, 18]

Table 1. Raman peaks identification for the different samples.

assignment of vibrational modes related with lithium ferrite and magnetite (Fe_3O_4) [20] was also made. In the particular case of lithium ferrate, it is interesting to focus that the vibrational band with higher intensity is centred at 125 cm^{-1} and the bands at 437 and 523 cm^{-1} show lower intensity. **Table 1** shows all vibration modes present for each sample.

In the morphological analysis of the samples (**Figure 5**), the increasing of the particle size is clearly visible from 100 nm for the sample heat-treated at 400°C to 4 μm approximately for the sample heat-treated at 1400°C.

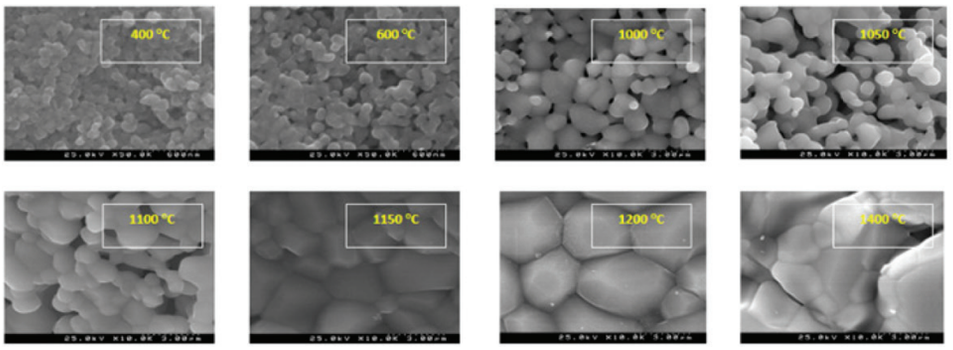


Figure 5. SEM micrographs for samples with heat treatments at 200, 400, 600, 1000, 1050, 1100, 1150, 1200 and 1400°C. Adapted from Refs. [5, 13, 14].

The aggregation of the spherical grains is quite evident, related to the Fe_2O_3, with the increase in the heat-treatment temperature. The formation of the $LiFe_5O_8$ phase shows a different microstructure, with prismatic grains clearly visible in the sample with heat treatment at 1150°C. In the sample treated at 1400°C, the formation of small grains attached to the prismatic grains is evident. As the shape of these grains is spherical, it could be attributed to the formation of Fe_2O_3, once this shape is the same as the one present in the samples treated at low temperatures. This aggregation to the prismatic particles also seems to appear in the sample treated at 1200°C. These results support the ones obtained by XRD and Raman measurements.

3.2. Electrical and dielectric measurements

The electrical measurements were performed on the samples heat-treated at temperatures between 400 and 1200°C. To interpret the temperature dependence of the dc conductivity, σdc data, the Arrhenius expression [21] has been used:

$$\sigma_{dc} = \sigma_0 exp\left(-\frac{E_{a(dc)}}{KT}\right) \quad (5)$$

Here σ_0 is a pre-exponential factor, $E_{a(\mathrm{dc})}$ the dc activation energy, K the Boltzmann constant and T the temperature. **Figure 6** shows the experimental data and the fit for all the treated samples.

The maximum of the conductivity is obtained for the sample heat-treated at 1100°C, which according to the XRD pattern only contains the $LiFe_5O_8$ crystal phase. For the other samples,

http://dx.doi.org/10.5772/110790

which also contain hematite, the conductivity increases with the temperature of heat treatment, and the activation energy decreases. This behaviour can be explained by the decrease in the hematite phase until the treatment temperature reaches 1100°C. The lower conductivity of the sample treated at 1200°C compared to the one treated at 1100°C can be related to the presence of lithium ferrate crystal.

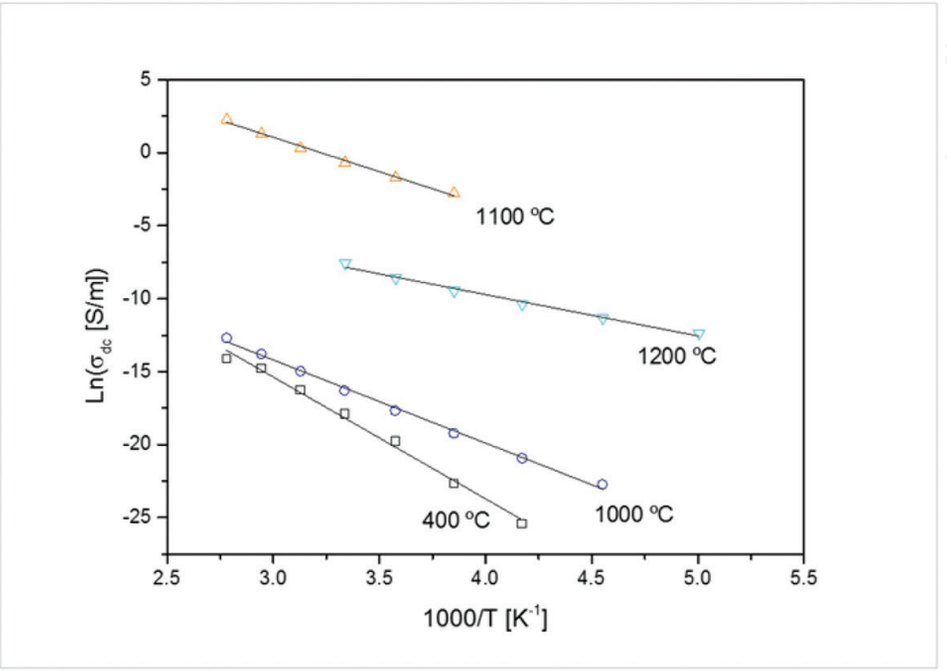


Figure 6. Log (σ_{dc}) versus 1000/T.

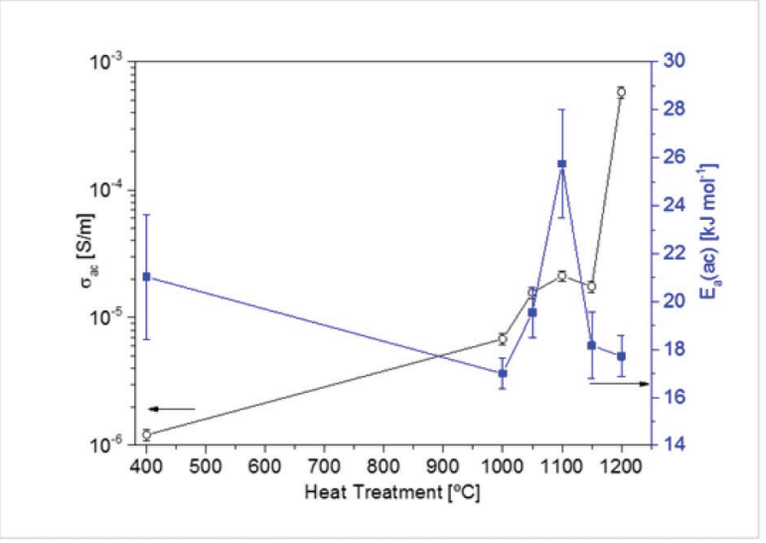


Figure 7. Dependence of the ac activation energy ($E_{a(ac)}$) and ac conductivity (σ_{ac}), at 300 K and 100 kHz, with heat-treatment temperatures.

Figure 7 shows the behaviour of the ac conductivity with the temperature of heat treatment. For samples treated at 1000, 1050, 1100 and 1150°C, there is a similar tendency between *ac* activation energy and conductivity. Similar to the dc conductivity variation of Eq. (3), the Arrhenius behaviour also fits correctly the ac data:

$$\sigma_{ac} = \sigma_0 exp\left(-\frac{E_{a(ac)}}{KT}\right) \tag{6}$$

Table 2 shows a comparison of the ac and dc activation energy for each sample.

Heating temperature (°C)	$E_{a(ac)} \pm \Delta E_{a(ac)}$ (kJ/mol)	$E_{a(dc)} \pm \Delta E_{a(dc)}$ (kJ/mol)
400	21.0 ± 2.6	69.4 ± 0.7
1000	17.0 ± 0.6	47.4 ± 0.5
1050	20 ± 1	
1100	26 ± 2	39.1 ± 1.6
1150	18 ± 1	
1200	17.7 ± 0.9	23.6 ± 0.2

Table 2. The *dc* and *ac* activation energies for the samples.

The dielectric measurements of C_p and R_p allowed us to calculate the real, ε′, and the imaginary, ε″, part of the complex permittivity using the equations [22]:

$$\varepsilon' = C_p \frac{d}{A\,\varepsilon_0} \tag{7}$$

$$\varepsilon'' = \frac{d}{\omega\, R_p\, \varepsilon_0} \tag{8}$$

Here d represents the sample thickness, A the electrode area, ε_0 the empty space permittivity and ω the angular frequency, respectively. These relations are only valid if $d \ll A$. The frequency dependence of the real part of the complex permittivity, ε′, and of the imaginary part of the complex permittivity, ε″, at constant temperature, $T = 300$ K, is shown in **Figure 8**.

According to **Figure 8**, the sample heat-treated at 1200°C presents the higher values of ε′, but the ε″ results are not suitable for their intended use due to their high losses, tanδ = 1.12 at 300 K and 1 kHz. On the other hand, the samples with heat treatments at 1050, 1100 and 1150°C have high dielectric constant and low losses at the same conditions of temperature and frequency: 0.86, 0.40 and 0.84, respectively.

Again, the behaviour is similar to that one observed with the other measurements. The increase in the complex permittivity with the treatment temperature is due to the structural and morphologic changes observed. This behaviour occurs for other ferrites [23, 24], where an increase in ε′ with the temperature of the heat treatment is observed. The crystallite size of the particles (**Figure 3**) influences the dielectric response, that is, the increase in the crystallite size, which is maximum for the samples treated at 1050, 1100, 1150 and 1200°C, leads to an increase in the dielectric constant.

http://dx.doi.org/10.5772/110790

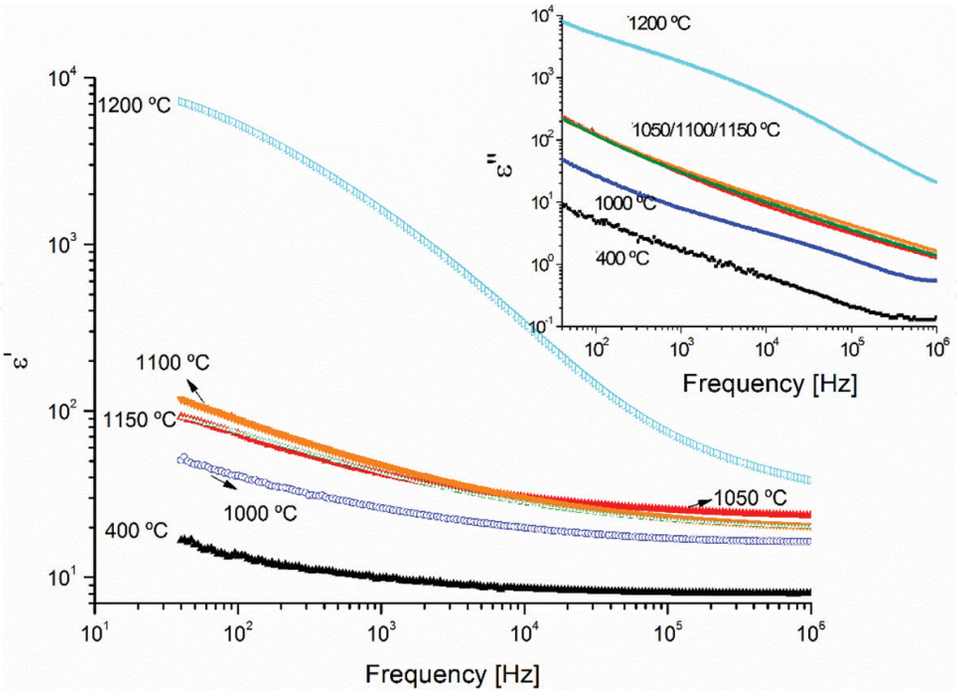


Figure 8. Frequency dependence of the complex permittivity, at T = 300 K [14].

The modulus formalism, where $M^* = 1/\varepsilon^*$, proposed by Macedo et al. [25] was used to study the dielectric response. **Figure 9** shows the frequency dependence of the imaginary part of the modulus (M″) for the sample that was heat-treated at 1050°C.

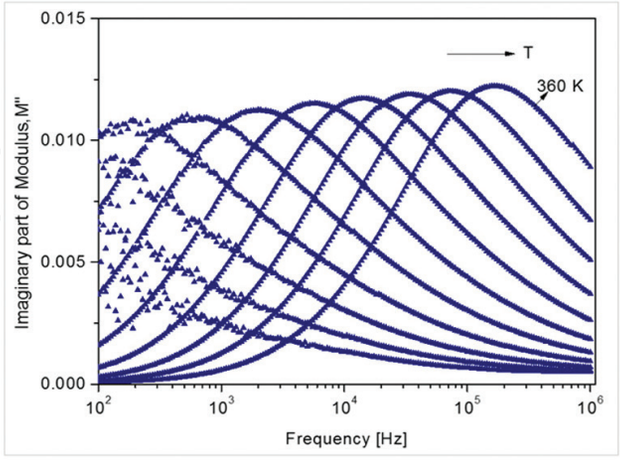


Figure 9. Imaginary part of the complex modulus, M″, for the sample treated at 1050°C, in the temperature range between 260 and 360 K, in steps of 10 K [14].

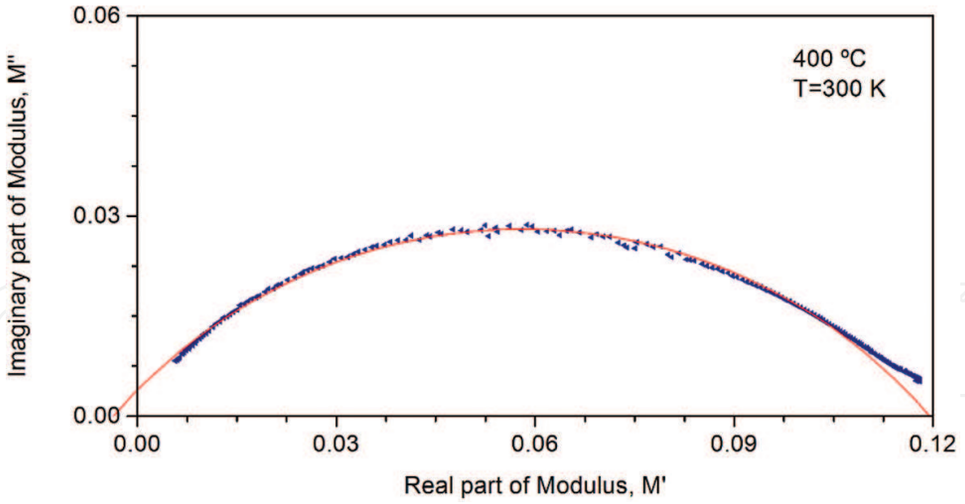


Figure 10. Nyquist plot fit for the sample heat-treated at 400°C for a temperature of measurement of 300 K [5].

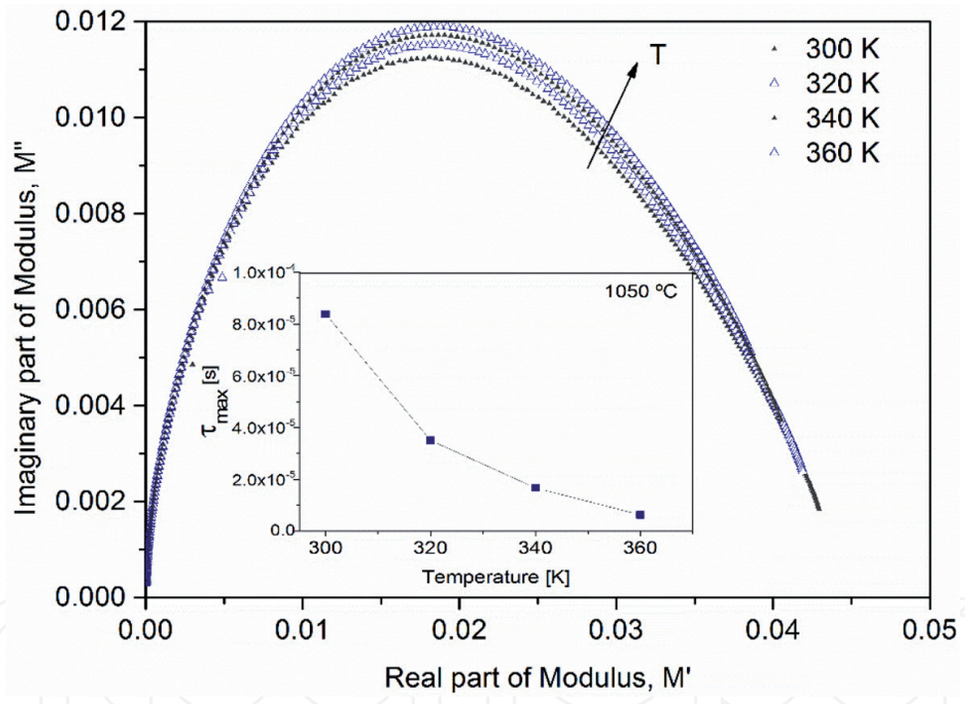


Figure 11. Nyquist plot for the sample treated at 1050°C for a range of temperatures between 300 and 360 K. Adapted from Ref. [14].

For all samples, a relaxation process is visible, as the one shown in **Figure 10**, which has a shape of a decentred semicircle, with its centre situated below the abscissa axis. **Figure 11** shows sample heat-treated at 1050°C, the evolution of the Nyquist plot with the temperature. From these results, the maximum of the relaxation time, τ_{max}, (**Figure 11** inset) shows a typical behaviour, that is, a decrease in the τ_{max} with increase in the temperature. This Cole-Cole analysis can also be made with the magnetic ac susceptibility data as the work presented by Wang and Seehra [26].

http://dx.doi.org/10.5772/110790

This profile indicates that the simple exponential decay, corresponding to a Debye relaxation, is inappropriate to describe the relaxation phenomena and should be replaced by an empirical model, such as Cole-Cole analysis [27]:

$$M^* = M_\infty + \frac{\Delta M}{1 + (iw\,\tau_M)^{1-\alpha_M}} \tag{9}$$

Eq. (9) represents a modification of the Debye equation since for $\alpha_M = 0$, the Debye model corresponding to a single relaxation time is recovered. In Eq. (9), α_M is a parameter between 0 and 1, which reflects the dipole interaction in the system; also M_∞ is the relaxed modulus; ΔM is the modulus relaxation strength; and τ_M is the relaxation time.

According to the values of the exponent parameter α_M, the system is a non-Debye, and for all samples, α_M decreases with the temperature. It decreases from about 0.56 to 0.50 in the sample treated at 400°C and from about 0.43 to 0.30 at 1200°C treated one. For modulus relaxation strength ΔM, the behaviour is similar to exponent parameter α_M, decreasing with temperature for each heat treatment (**Figure 12**).

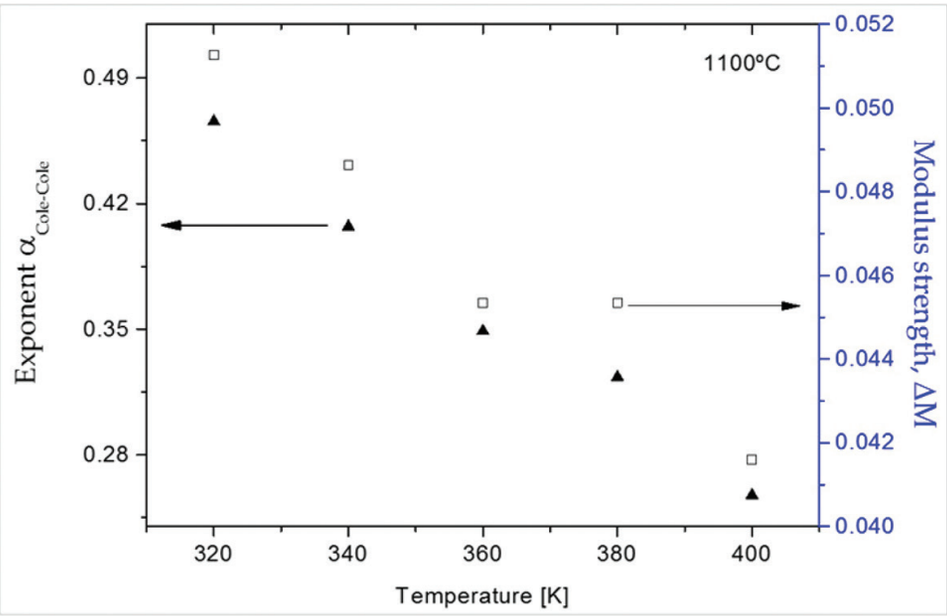


Figure 12. Temperature dependence of the $\alpha_{Cole-Cole}$ parameter and ΔM for sample heat-treated at 1100°C [14].

The relaxation frequency, $f_{max} = \frac{1}{2\pi\tau}$, can be expressed by the Arrhenius law, where

$$f_{max} \propto exp\left(-\frac{E_a}{KT}\right) \tag{10}$$

In Eq. (10), E_a is the activation energy for the relaxation process. The logarithmic representation of the relaxation frequency versus the inverse temperature, the relaxation map, allows to obtain the activation energy (**Figure 13**). Also in this process, the activation energy decreases with the temperature of the treatment unless for the samples treated at 1050, 1100 and 1150°C which increases. This may be related to structural changes, since at this heat treatment temperature only the crystalline phase of lithium ferrite is present. The same tendency as the one

observed in the ac conductivity regime, in the samples with only one crystal phase, $LiFe_5O_8$. **Table 3** resumes all the activation energies of the relaxation process.

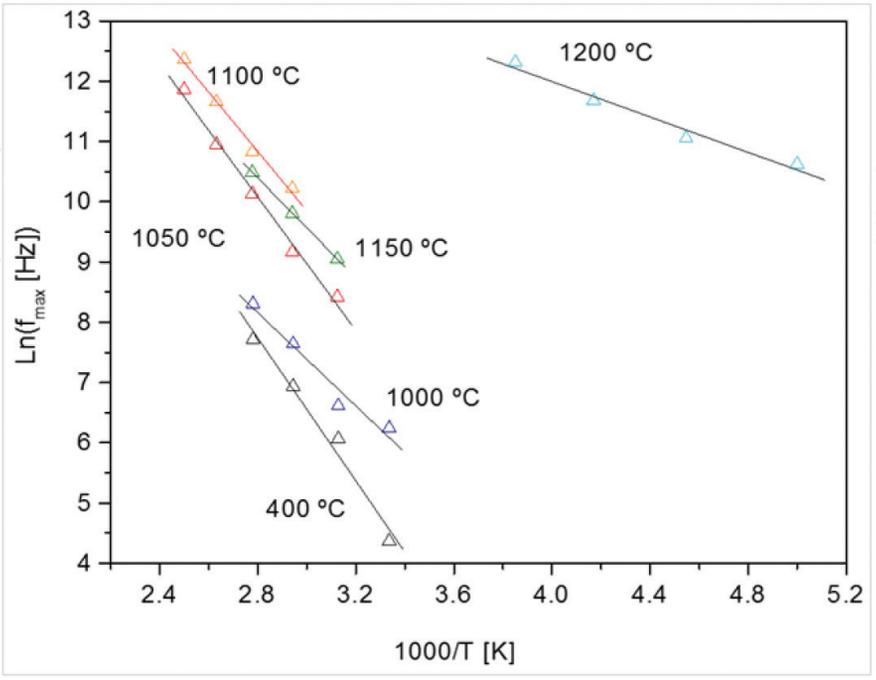


Figure 13. Ln (f_{max}) versus 1000/T [14].

Heat-treated sample (°C)	$E_a \pm \Delta E_a$ (kJ/mol)
400	21 ± 3
1000	32 ± 2
1050	46.0 ± 0.8
1100	37.3 ± 0.8
1150	34.45 ± 0.01
1200	12.2 ± 0.7

Adapted from Ref. [14].

Table 3. The activation energy for the relaxation process for all the samples investigated here.

3.3. Magnetic measurements

The magnetic measurements were performed on the samples heat-treated at 200, 400, 600, 1000, 1050, 1100, 1150, 1200 and 1400°C. Initially, the measurements were performed in ZFC condi-

tions with an applied magnetic field (*B*) of 0.1 T, from 5 K up to 300 K. At 300 K, magnetization (*M)* versus *B* measurements were performed. Then, FC measurements were performed from 300 K down to 5 K under the magnetic field of 0.1 T. Again, at 5 K, *M* versus *B* measurements were also performed. This experimental sequence is important to explain why after the M versus B at 300 K, an increase of magnetic susceptibility in the FC curves is observed, which can be ascribed to the remnant magnetization of the sample (**Figure 14a** and **b**).

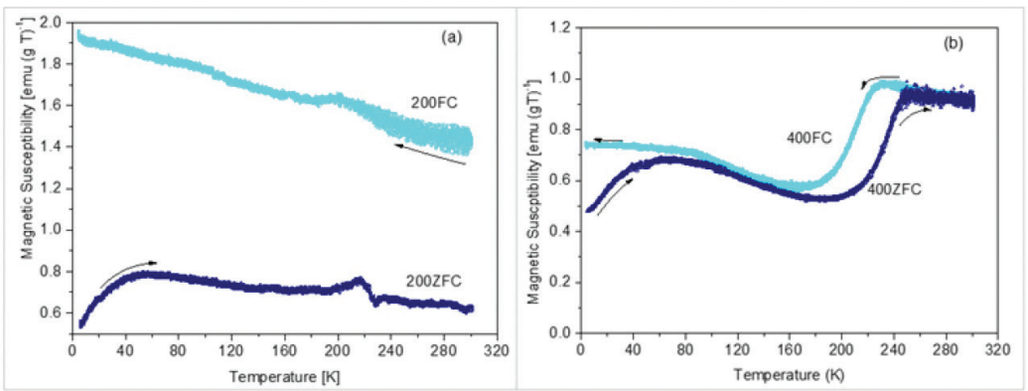


Figure 14. Magnetic susceptibility versus temperature, recorded under zero field cooled (ZFC) and field cooled (FC) sequences with *B* = 0.1 T, between 5 and 300 K, for the samples with a heat treatment of 200°C (a) and 400°C (b). Adapted from Ref. [13].

In **Figure 14a**, in the sample treated at 200°C, the results of the magnetic susceptibility recorded under ZFC and FC show the presence of a blocking temperature (T_B) between 50 and 70 K. This blocking temperature was observed with the translation of the FC curve into the ZFC curve, where T_B is the temperature which separates the FC and ZFC curves. **Figure 14b**, shows that in the sample treated at 400 °C, T_B is slightly higher, around 70 K, than in the sample treated at 200 °C. This difference can be related to the particles size, which is higher for the sample heat-treated at 400°C (**Figure 5**). The dependence of the magnetic susceptibility on temperature is shown in **Figure 15**.

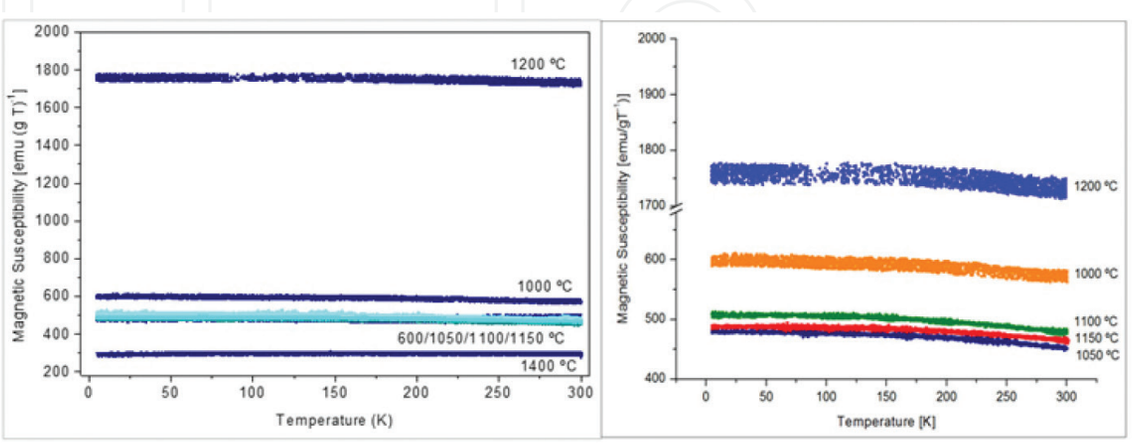


Figure 15. Magnetic susceptibility versus temperature, recorded under field cooled (FC) with an applied magnetic field of 0.1 T, between 5 and 300 K. Adapted from Ref. [13].

With the exception of samples treated at 200 and 400°C, a decrease in the magnetic susceptibility with increase in the temperature of measurement is observed in the remaining samples. This behaviour of the dependence of the susceptibility with the temperature was expected because it is characteristic of ferromagnetic materials. This feature will change to a non-magnetic order (paramagnetic characteristic) above Curie temperature, which is, according to Iliev et al. [8], about 893 K for lithium ferrite This property was not observed because in our experimental procedure the maximum temperature of measurement was 300 K (**Figure 15**). The sample heat-treated at 1200°C shows the highest magnetic susceptibility.

As noted earlier, the XRD diffraction patterns of the samples heat-treated at 1050, 1100 and 1150°C are characteristic of a single lithium ferrite phase (**Figure 2**). The SEM micrographs of these samples (**Figure 5**) show an increase in the grain size, changing from about 100 nm for sample treated at 400°C to 4 μm for sample treated at 1400°C. This promotes the increase in the probability of the random distribution of magnetic moments and therefore an increase in the soft magnetic type response.

Figure 16a and **b** shows the magnetization versus applied field, measured at 5 K, for all the samples. It should be noticed that **Figure 16b** is presented only to show a better graphical visualization of the magnetization of the samples treated between 1000 and 1200°C. The samples heat-treated at 200 and 400°C present a low magnetization, due to the fact that the major phase is antiferromagnetic α-Fe_2O_3.

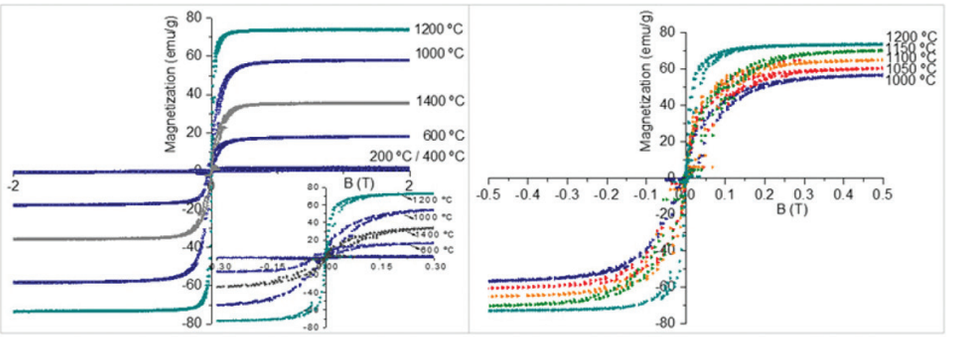


Figure 16. Magnetic hysteresis curves (T = 5 K). Adapted from Ref. [13].

In the literature [28, 29], the magnetization of the lithium ferrite is around 60 emu/g, which is rather lower than the one obtained in this work (**Figure 16**). In these samples, the generation of the lithium ferrite phase takes to the decrease in the contribution of the α-Fe_2O_3 particles with low magnetization. XRD and Raman results confirm that the samples heat-treated at temperatures between 1000 and 1200°C have the ordered phase α-$LiFe_5O_8$ as the major phase. Very likely, this ordered ferrite phase is developed from the thermal-activated reaction between α-Fe_2O_3 and "free" lithium ions present in the lattice, suggesting the existence of some amorphous phase, whose amount decreases with the increase in the heat-treatment temperature. The presence of this lithium ferrite phase also promotes the increase in the magnetization (**Figure 16**), showing a maximum of 73 emu/g, for the sample treated at 1200°C, which is a

similar value to the one obtained by Singhal [30] on lithium ferrite prepared by aerosol route. This high magnetization is attributed to the formation of Fe_3O_4 (M_s = 92 emu/g [31]) as proved by XRD results. For this sample, the minimum magnetic field that saturates the sample is around 0.1 T, meaning that this sample magnetizes easily [13]. The further increase in the heat-treatment temperature of 1400°C also promotes the development of hematite, α-Fe_2O_3 (**Figure 2**), whose magnetization of saturation is around ~10 emu/g [32, 33]. This should be the reason for the observed decrease in magnetization from sample treated at 1200 (73 emu/g) to sample treated at 1400°C (30 emu/g) (**Figure 16**). Moreover, the contribution of Li_2FeO_3 to the absolute magnetization should be lower than the one of $LiFe_5O_8$ in accordance with Hessien et al. [34] who states that the increase in the molar ratio between Fe^{3+} and Li^+ leads to lower magnetization values.

Shirsath et al. [35] have studied this particular type of ferrite, prepared using also nitrates as initial materials but following a sol-gel method. Comparing their results with ours and taking into account the fact that the followed method was the solid-state route, the magnitudes of the magnetization for our samples are higher, nearly 73 and 55 emu/g for the sample heat-treated at 1200 and 1000°C respectively. The values for the same treatment temperatures, obtained by Shirsath et al. through the sol-gel method, are around 55 and 45 emu/g, respectively, and related to the particle size. In the referred work, as the particle size increases, the magnetization decreases. For the sample treated at 600°C, which has also a large amount of hematite (**Figure 2**), the results are similar for both methods.

4. Conclusions

The $LiFe_5O_8$ crystal phase was obtained using nitrates as raw materials by an easy and relatively inexpensive route. From the structural and morphological results, the lithium ferrite crystal phase obtained is the ordered one, α-$LiFe_5O_8$, and is mostly present in the samples with thermal treatment from 1000 to 1200°C. Heat treatments above 1150°C promote the formation of the Li_2FeO_3 and Fe_3O_4 crystal phases. Spherical grains related to α-Fe_2O_3 were detected in the sample heat-treated at 1400°C. The formation of lithium ferrite phases leads to a different microstructure (prismatic grains), whose size increases with the increase in heat-treatment temperature, obtaining a maximum for 1200°C. In the sample treated at 1400°C, SEM micrograph shows modification in the surface that is related to the lithium ferrate crystal phase and the appearance of α-Fe_2O_3.

Electrical measurements suggest that the samples with heat treatments at 1000, 1050 and 1150°C have a good dielectric response; however, the sample treated at 1100°C is more suitable for application in electronic devices.

Magnetic analysis confirms that the presence of α-Fe_2O_3 that leads to a decrease in the magnetization as a function of the applied field. The presence of α-$LiFe_5O_8$ and Fe_3O_4 contributes to the maximum magnetization magnitude observed (73 emu/g at the sample treated at 1200°C). The magnetic susceptibility as a function of temperature has a maximum value of nearly 1750 emu $(gT)^{-1}$ for the sample treated at 1200°C confirming that this sample has a good magnetic response.

Acknowledgements

This work was financed by FEDER funds through the COMPETE 2020 Programme and National Funds through FCT—Portuguese Foundation for Science and Technology under the project UID/CTM/50025/2013. S. Soreto Teixeira also acknowledges to the FCT for a Ph D. Grant SFRH/BD/105211/2014.

Author details

Sílvia Soreto*, Manuel Graça, Manuel Valente and Luís Costa

*Address all correspondence to: silvia.soreto@ua.pt

Department of Physics, I3N - University of Aveiro, Aveiro, Portugal

References

[1] Louh R-F, Reynolds TG, Buchanan RC. Ferrite Ceramics. In: Buchanan RC, editor. Ceramic Materials for Electronics. first ed. New York: Dekker, Marcel; 1986. p. 323–76.

[2] Pullar RC. Hexagonal ferrites: a review of the synthesis, properties and applications of hexaferrite ceramics. Prog Mater Sci [Internet]. Elsevier Ltd; 2012 Sep [cited 2014 Jun 3];57(7):1191–334. Available from: http://linkinghub.elsevier.com/retrieve/pii/S0079642512000369

[3] Rubinger CPL, Gouveia DX, Nunes JF, Salgueiro CCM, Paiva JAC, Graça MPF, et al. Microwave dielectric properties of $NiFeO_4$ nanoparticles ferrites. Microw Opt Technol Lett. 2007;49(6):1341–3.

[4] Snelling EC. Soft ferrites Properties and Applications. second ed. London: Butterwoeth & Co. (Publishers) Ltd; 1988.

[5] Teixeira SS, Graça MPF, Costa LC. Dielectric, morphological and structural properties of lithium ferrite powders prepared by solid state method. J Non Cryst Solids [Internet]. Elsevier B.V.; 2012 Aug [cited 2014 Jun 24];358:1924–9. Available from: http://linkinghub.elsevier.com/retrieve/pii/S0022309312003183

[6] Gingasu D, Mindru I, Patron L, Stoleriu S. Synthesis of lithium ferrites from polymetallic carboxylates. J Serbian Chem Soc. 2008;73(10):979–88.

[7] Wolska E, Piszora P, Nowicki W, Darul J. Vibrational spectra of lithium ferrites: infrared spectroscopic studies of Mn-substituted $LiFe_5O_8$. Int J Inorg Mater. 2001;3:503–7.

[8] Iliev MN, Ivanov VG, Todorov ND, Marinova V, Abrashev MV, Petrova R, et al. Lattice dynamics of the α and β phases of $LiFe_5O_8$. Phys Rev B [Internet]. 2011 May [cited 2014 Jun 24];83:174111-1–7. Available from: http://link.aps.org/doi/10.1103/PhysRevB.83.174111

[9] Ahniyaz A, Fujiwara T, Song S, Yoshimura S. Low temperature preparation of β-$LiFe_5O_8$ fine particles by hydrothermal ball milling. Solid State Ionics. 2002;151:419–23.

[10] Dey S, Roy A, Das D, Ghose J. Preparation and characterization of nanocrystalline disordered lithium ferrite by citrate precursor method. J Magn Magn Mater [Internet]. 2004 Mar [cited 2014 Jun 24];270(1–2):224–9. Available from: http://linkinghub.elsevier.com/retrieve/pii/S030488530300711X

[11] Jović NG, Masadeh AS, Kremenovic AS, Antic BV, Blanusa JL, Cvjeticanin ND, et al. Effects of thermal annealing on structural and magnetic properties of lithium ferrite nanoparticles. J Phys Chem C [Internet]. 2009 [cited 2014 Jun 24];113:20559–67. Available from: http://pubs.acs.org/doi/abs/10.1021/jp907559y

[12] Widatallah HM, Berry FJ. The influence of mechanical milling and subsequent calcination on the formation of lithium ferrites. J Solid State Chem. 2002;164:230–6.

[13] Teixeira SS, Graça MPF, Costa LC, Valente MA. Study of the influence of thermal treatment on the magnetic properties of lithium ferrite prepared by wet ball-milling using nitrates as raw material. Mater Sci Eng B [Internet]. 2014 Aug [cited 2014 Jun 24];186:83–8. Available from: http://linkinghub.elsevier.com/retrieve/pii/S0921510714000762

[14] Teixeira SS, Graça MPF, Costa LC. Dielectric and structural properties of lithium ferrites. Spectrosc Lett [Internet]. 2014 May 28 [cited 2014 Jun 24];47(5):356–62. Available from: http://www.tandfonline.com/doi/abs/10.1080/00387010.2013.840316

[15] Jones FW. The Measurement of Particle Size by the X-Ray Method. R Soc London A. 1938;166(924):16–43.

[16] Patterson AL. The Scherrer formula for I-Ray particle size determination. Phys Rev. 1939;56:978–82.

[17] Devesa S, Graça MP, Henry F, Costa LC. Microwave dielectric properties of (Bi1-xFex) NbO_4 ceramics prepared by the sol–gel method. Ceram Int. 2015;41(6):8186–90.

[18] Cook W, Manley M. Raman characterization of a- and b-$LiFe_5O_8$ prepared through a solid-state reaction pathway. J Solid State Chem [Internet]. Elsevier; 2010;183(2):322–6. Available from: http://dx.doi.org/10.1016/j.jssc.2009.11.011

[19] Nasibulin AG, Simas R, Jiang H, Tian Y, Mudimela PR, Shandakov SD, et al. Simple and rapid synthesis of ambient conditions α-Fe_2O_3 nanowires under ambient conditions. Nano Res. 2009;2:373–9.

[20] Shebanova ON, Lazor P. Raman spectroscopic study of magnetite ($FeFe_2O_4$): a new assignment for the vibrational spectrum. J Solid State Chem. 2003;174:424–30.

[21] Graça MPF, Valente MA, Da Silva MF. The electric behavior of a lithium-niobate-phosphate glass and glass-ceramics. J Mater Sci. 2006;41:1137–44.

[22] Jonscher AK. Dielectric Relaxation in Solids. London: Chelsea Dielectrics Press; 1983.

[23] Shitre AR, Kawade VB, Bichile GK, Jadhav KM. X-ray diffraction and dielectric study of $CoCo_{1-x}Cd_xFe_{2-x}Cr_xO_4$ ferrite system. Mater Lett. 2002;56:188–93.

[24] Singh AK, Goel TC, Mendiratta RG, Thakur OP, Prakash C. Dielectric properties of Mn-substituted Ni–Zn ferrites. J Appl Phys. 2002;91:6626–30.

[25] Macedo BP, Moynihan CT, Bose R. Role of ionic diffusion in polarization vitreous conductors. Phys Chem Glasses. 1972;13:171–179.

[26] Wang Z, Seehra MS. Ising-like chain magnetism, Arrhenius magnetic relaxation, and case against 3D magnetic ordering in β-manganese phthalocyanine ($C_{32}H_{16}$ MnN_8). J Phys Condens Matter [Internet]. IOP Publishing; 2016;28(136002):1–9. Available from: http://stacks.iop.org/0953-8984/28/i=13/a=136002?key=crossref.5ce814db016d8c3680972e0aa65d1762

[27] Cole KS, Cole RH. Dispersion and absorption in dielectrics I. alternating current characteristics. J Chem Phys. 1941;9:341–51.

[28] Jovic N, Antic B, Goya GF, Spasojevic V. Magnetic properties of lithium ferrite nanoparticles with a core/shell structure. Curr Nanosci. 2012;8(5):1–8.

[29] Verma S, Joy PA, Verma S, Joy PA. Magnetic properties of superparamagnetic lithium ferrite nanoparticles. J Appl Phys. 2005;98(124312):1–9.

[30] Singhal S. Cation distribution in lithium ferrite ($LiFe_5O_8$) prepared via aerosol route. J Electromagn Anal Appl. 2010;2(1):51–5.

[31] Mikhaylova M, Kim DK, Bobrysheva N, Osmolowsky M, Semenov V, Tsakalakos T, et al. Superparamagnetism of magnetite nanoparticles: dependence on surface modification. Langmuir. 2004;20:2472–7.

[32] Wang WW, Zhu YJ, Ruan ML. Microwave-assisted synthesis and magnetic property of magnetite and hematite nanoparticles. J Nanoparticle Res. 2007;9:419–26.

[33] Skomski R, Coey JMD. Permanent Magnetism. Taylor & Francis, editor. Bristol: Institute of Physics Publishing Ltd.; 1999.

[34] Hessien MM. Synthesis and characterization of lithium ferrite by oxalate precursor route. J Magn Magn Mater. 2008;320:2800–7.

[35] Shirsath SE, Kadam RH, Gaikwad AS, Ghasemi A, Morisako A. Effect of sintering temperature and the particle size on the structural and magnetic properties of nanocrystalline $Li_{0.5}Fe_{2.5}O_4$. J Magn Magn Mater [Internet]. Elsevier; 2011;323:3104–8. Available from: http://dx.doi.org/10.1016/j.jmmm.2011.06.065